Fragmentation of the adenine and guanine molecules induced by electron collisions

B. F. Minaev, M. I. Shafranyosh, Yu. Yu Svida, M. I. Sukhoviya, I. I. Shafranyosh, G. V. Baryshnikov, and V. A. Minaeva

Citation: The Journal of Chemical Physics **140**, 175101 (2014); doi: 10.1063/1.4871881
View online: http://dx.doi.org/10.1063/1.4871881
View Table of Contents: http://scitation.aip.org/content/aip/journal/jcp/140/17?ver=pdfcov
Published by the AIP Publishing

Fragmentation of the adenine and guanine molecules induced by electron collisions

B. F. Minaev,[1,2,a)] M. I. Shafranyosh,[3] Yu. Yu Svida,[3] M. I. Sukhoviya,[3] I. I. Shafranyosh,[3] G. V. Baryshnikov,[1] and V. A. Minaeva[1]
[1]*Bohdan Khmelnitsky National University, 18031 Cherkasy, Ukraine*
[2]*Tomsk State University, 634050 Tomsk, Russian Federation*
[3]*Uzhgorod National University, 88000 Uzhgorod, Ukraine*

(Received 2 February 2014; accepted 8 April 2014; published online 2 May 2014)

Secondary electron emission is the most important stage in the mechanism of radiation damage to DNA biopolymers induced by primary ionizing radiation. These secondary electrons ejected by the primary electron impacts can produce further ionizations, initiating an avalanche effect, leading to genome damage through the energy transfer from the primary objects to sensitive biomolecular targets, such as nitrogenous bases, saccharides, and other DNA and peptide components. In this work, the formation of positive and negative ions of purine bases of nucleic acids (adenine and guanine molecules) under the impact of slow electrons (from 0.1 till 200 eV) is studied by the crossed electron and molecular beams technique. The method used makes it possible to measure the molecular beam intensity and determine the total cross-sections for the formation of positive and negative ions of the studied molecules, their energy dependences, and absolute values. It is found that the maximum cross section for formation of the adenine and guanine positive ions is reached at about 90 eV energy of the electron beam and their absolute values are equal to 2.8×10^{-15} and 3.2×10^{-15} cm^2, respectively. The total cross section for formation of the negative ions is 6.1×10^{-18} and 7.6×10^{-18} cm^2 at the energy of 1.1 eV for adenine and guanine, respectively. The absolute cross-section values for the molecular ions are measured and the cross-sections of dissociative ionization are determined. Quantum chemical calculations are performed for the studied molecules, ions and fragments for interpretation of the crossed beams experiments. © *2014 AIP Publishing LLC*. [http://dx.doi.org/10.1063/1.4871881]

I. INTRODUCTION

Ribonucleic and deoxyribonucleic acids (RNA and DNA) are composed of two antiparallel strands of repeated sugar-phosphate units which are hydrogen-bond bound together through the four nucleobases, covalently linked to the sugar moiety (deoxyribose) of the backbone. Any ionizing lesion of nucleobases can induce mutagenic and genotoxic damages in RNA and DNA, including double-strand breaks.[1] These lesions are induced by secondary electrons, generated by the primary ionizing radiation; below 20 eV, they are the most abundant of these secondary active species.[2] Therefore, a detailed investigation of the secondary low-energy electrons action is of crucial importance for understanding the main fundamental mechanisms by which the ionizing radiation damages the DNA components. In order to reach such understanding, the low-energy electron impact on basic DNA components has been investigated by various techniques[1–4] including the recent activity.[5–9] It was shown that the impact of 5–150 eV electrons on dry DNA thin films produces both single and double-strand breaks.[4] The electron energy dependence of the yields of these breaks exhibited the strong resonance features with a maximum between 8 and 10 eV[4–6] close to ionization potentials. These authors also concluded that most of the strand breaks below 15 eV are initiated by resonant electron attachment to the various components of DNA, followed by the decay of the local transient anion in dissociative channels.[2–11]

Not only the number of emitted electrons is relevant, but also their energy spectrum, because, it has been shown that low energy electrons (below ionization threshold) can also produce damage to biomolecules by dissociative electron attachment (DEA).[2,3] In the DEA processes, the excess electrons generally occupy the lowest unoccupied molecular orbitals (LUMO) of the DNA nucleobases and create transient anions.[5] Attachment of the low-energy electrons not only causes the strand breaks in DNA, but also induces fragmentation of the DNA bases. The pyrimidine bases as the representative components of biological species have been extensively studied,[6–10] both experimentally and theoretically. The progress in fundamental aspects of multidisciplinary studies of low-energy electron-induced damage in biomolecules has been reviewed recently.[6] It is known that even under high vacuum conditions, DNA still contains 2–3 water molecules per nitrogeneous base pair.[1–4] That is why the pure nucleobases in molecular beam experiments are so important for the basic molecular backgrounds of the radiative damage studies. It is necessary to stress that the important channel to generate free low-energy electrons is the interatomic Coulomb decay

a)Authors to whom correspondence should be addressed. Electronic addresses: bfmin@rambler.ru and boris@theochem.kth.se.

(ICD) which takes places predominantly in water molecules surrounding DNA.[12–14] This means that at external irradiation impact the electron excitation of inner valence vacancy states being possible to decay by Auger process that knocks out secondary low-energy electrons[13] in the DNA molecule itself or in the nearby water molecules.

The DEA parameters for an isolated basic constituent are expected to be strongly affected within condensed phase of DNA or in living cells by the local environment of the molecule, thus changing the magnitude of the measured cross-section.[2,3] Therefore, the pure electron scattering experiment under high vacuum is quite important to comprehend the mechanism of slow electron interaction with nucleobasis and the crossed electron and molecular beams techniques are widely used now.[6–9]

In previous works,[6,8–10] the processes of excitation by slow electrons of nucleic acid bases of the pyrimidine type molecules, such as cytosine, uracil, and thymine in the gas phase have been investigated. The present work is devoted to the purine type molecules, adenine, and guanine.

II. METHODS OF THE STUDY

A. Experimental technique

The experiments are performed by using the setup with the crossed molecular and electron beams, which has been used in the previous studies of ionization processes in pyrimidine derivatives of nitrogeneous bases of nucleic acids.[6,8–10] In the present work, the beam of adenine or guanine molecules is generated utilizing an effusive thermal multichannel source with a system of collimating slits.[6] The studied purine bases of 99% purity were obtained from the Sigma–Aldrich company (USA). To exhale the molecular vapor and create a beam the necessary temperature of the source found experimentally does not exceed 410 K which is lower than the thermolysis limit for the studied molecules. We have ruled out any thermal decomposition of adenine in the oven at this temperature, because no changes in the relative anion efficiency curves have been observed in Ref. 11 even for 430–470 K in a similar effusive source. This also indicates a small contribution of vibrationally excited neutral adenine molecules to the measured anion efficiency curves.[11]

The beam of adenine or guanine is crossed with an electron beam which is introduced in a special type of ion source. The energy spread resolution of the electron beam is approximately 0.3 eV at an electron current of 5×10^{-6} A. The molecules travel through the region of interaction with electrons and experience multiple collisions. The effusive source consists of a copper hollow cylinder container with the studied sample, a resistive heater with calibrated thermocouple sensor and thermal screens. At the ends of the cylinder the effusive device is installed which contains 100 channels (1.5×1.5 mm^2 area each). At the other side the container is locked by a hermetic cover, on which inner surface the temperature sensors are placed.[6]

As a source of electrons, the five-electrodes electron gun with a tungsten cathode is used.[9] The first electrode operates at a small negative potential,[9] which blocks the low-energy part of the beam from the cathode. The electrons of the beam after their passage through the collision region are trapped by a Faraday cup having a negative potential. The measurements were performed at an electron beam current of 5×10^{-6} A and an FWHM energy spread of $\Delta E_{1/2} \sim 0.3$ eV. The electron gun operates in a longitudinal magnetic field with an induction of $B = 1.2 \times 10^{-2}$ T. Note that in the presence of the longitudinal magnetic field, the electron beam move along the troichoid trajectories with the lengths which exceed the linear sizes of the cross sections of the electron and molecular beams. Due to this effect the maximal path length of the fast electrons (with energy of 90 eV) increases slightly by a factor of 1.01, but for the slow electrons (with energy of 5 eV) the path length increases by a factor of 1.25 under the conditions of our experiment. (These estimations are done for the above-mentioned magnetic field induction and the diameter of diaphragms of the beam). Calibration of the electron energy scale is performed by the resonance peak of the SF_6^- ions formation, which signal is established as the zero origin of the electron energy. (The collision chamber was filled with the SF_6 gas at a pressure of $1.3\ 10^{-3}$ Pa).

The ions created in the crossing region of the molecular and electron beams are drawn out by electric field and guided to mass-spectroscopic analysis. The *m/z* ratio is measured by mass-spectrometer MI-1201 for recording the mass spectra and by specially designed spectrometer with deviation of ions by 180° for measuring the energy dependence of the total ionization cross-sections.

Experimental measurements are preformed in two steps: at the first step, the mass spectra are recorded and identified at the electron beam energy of 95 eV; at the second stage, the energy dependence of the ionization cross-sections for the guanine and adenine molecules is studied. Absolute values of partial ionization cross-sections are determined by their calibration with respect to the absolute values of the total ionization cross-sections. The presented cross-section values are obtained by the five averaged measurements. The relative error of the energy dependence measurements for the ionization cross-sections is equal to 12%, for their absolute values—21%.

The setup developed makes it possible to measure the molecular beam intensity and determine the energy dependences and absolute values of total cross sections for the formation of positive and negative ions of the adenine and guanine molecules. It is found that the maximum cross-section for the formation of positive ions is reached at energy of about 90 eV.

B. Computational strategy

The adenine and guanine molecules, their cations and anions are calculated in their ground states by the density functional theory (DFT) with complete geometry optimization by the finding of global minima on their potential energy hypersurfaces (PEHs). The gradients of the PEHs with respect to all internal coordinates are minimized and the corresponding second derivative matrices (Hessians) are calculated with the B3LYP functional[15] in the 6-31G basis set.[16] The doublet states of the ions are calculated by the spin unrestricted

DFT method.[16] On this background, the vibrational analysis is performed and all vibrational frequencies are found to be real which corresponds to a criterion of the true equilibrium structure. Comparison of the equilibrium bond lengths in the neutral and ionized molecules indicates the corresponding changes in the force constants which show the most probable routes of fragmentation upon ionization. For fragmentation of molecular ion the simultaneous cleavage of at least two chemical bonds is necessary. Dissociation of the ion into two fragments is predicted by analysis of possible sums of the bond lengths changes along all various fragmentation routes. All possible double and triple cleavages of chemical bonds are considered. For explanation of the observed mass spectra for the adenine and guanine molecules, we proposed that the most probable cleavages have to be in those places, where the sums of two bond lengths changes are the largest upon ionization. The analysis and comparison with experiment indicate that the simultaneous cleavages of three chemical bonds are less probable.

The starting geometry is obtained first by the semi-empirical self-consistent field (SCF) molecular orbital (MO) methods with the AM1 approximation.[17] We also use AM1 and PM3 results for some preliminary analysis including configuration interaction (CI) calculations for the doublet excited states of the ions. For anions, the energy of the dissociation products is estimated with account of the zero-vibration correction. All calculations were performed with the GAUSSIAN 09 program package.[16]

III. RESULTS AND DISCUSSION

A. Positive ions

Mass spectra of adenine and guanine at the 95 eV energy of the bombarding electrons are presented in Figures 1 and 2, respectively (on the ordinate axis the current of produced ions is given in arbitrary units). In general features, the obtained spectra are similar to those presented in Refs. 18–22, but there are some differences. These concern intensity distribution in spectral lines and also the number of lines. First of all, these distinctions are determined by the differences in the processes of the ion generation in the excited states. For example, in Refs. 18 and 20, such ions are produced by electron impact, in Ref. 19—by photoionization, in Ref. 23, the mass spectrum of adenine is induced by heavy ions. One needs also to account such important factor as the temperature of the substances heating.

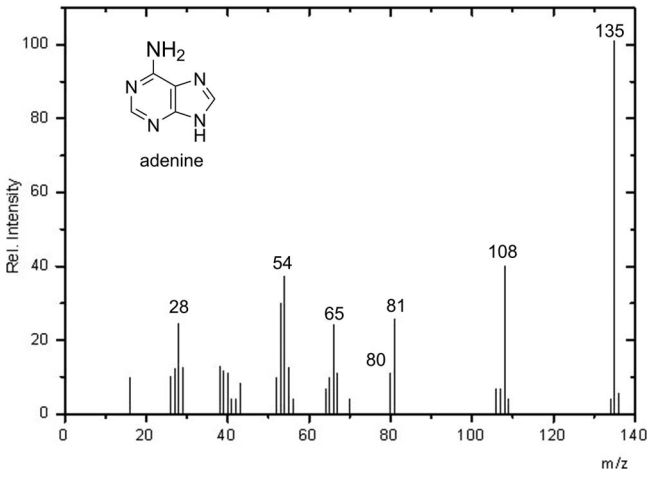

FIG. 1. Mass spectrum of adenine measured with 95 eV electron energy.

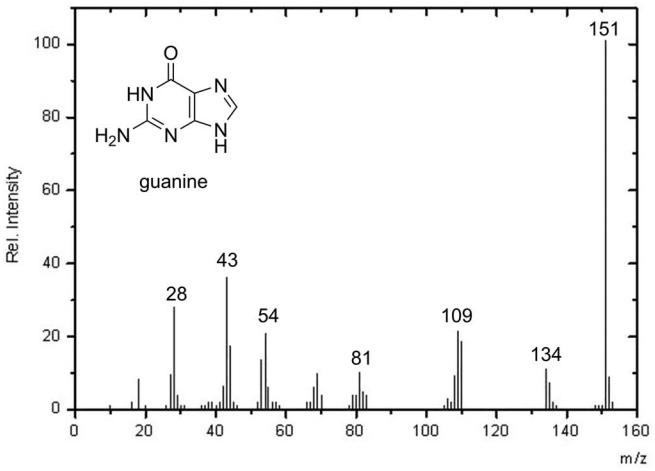

FIG. 2. Mass spectrum of guanine measured with 95 eV electron energy.

Identification of the mass spectra is presented in Table I (adenine) and Table II (guanine). The common features of the presented mass spectra are the following: (1) the presence of the most intense lines which corresponds to the

TABLE I. The absolute cross-sections values for the positive ionic fragments formation of adenine.

m/z, amu	Ionic fragments	σ, 10^{-15} cm^2
27	CHN^+	0.07
28	CH_2N^+	0.15
29	CH_3N^+	0.06
38	C_2N^+	0.08
39	C_2HN^+	0.07
40	$C_2H_2N^+$,CN_2^+	0.07
41	CHN_2^+	0.02
42	$CH_2N_2^+$	0.035
43	$CH_3N_2^+$	0.07
52	$C_2N_2^+$	0.05
53	$C_2HN_2^+$	0.18
54	$C_2H_2N_2^+$	0.23
55	$C_2H_3N_2^+$	0.08
64	$C_3N_2^+$	0.035
65	$C_3HN_2^+$	0.05
66	$C_3H_2N_2^+$	0.14
67	$C_3H_3N_2^+$	0.07
70	$C_2H_4N_3^+$	0.035
80	$C_3H_2N_3^+$	0.07
81	$C_3H_3N_3^+$	0.16
106	$C_4H_2N_4^+$	0.04
107	$C_4H_3N_4^+$	0.035
108	$C_4H_4N_4^+$	0.25
134	$C_5H_4N_5^+$	0.02
135	$C_5H_5N_5^+$	0.7
136		0.03

TABLE II. The absolute cross-sections values for the positive ionic fragments formation of guanine.

m/z, amu	Ionic fragments	σ, 10^{-15} cm^2
27	CHN^+	0.08
28	CO^+, CH_2N	0.23
42	CNO^+	0.08
43	$CH_3N_2^+$, $CHNO^+$	0.33
44	$CH_4N_2^+$, CH_2NO^+	0.17
53	$C_2H_3N_2^+$	0.12
54	$C_2H_2N_2^+$	0.2
55	$C_2H_2NO^+$	0.05
68	$C_2H_2N_3^+$	0.04
69	$C_2H_3N_3^+$	0.08
81	$C_3H_3N_3^+$	0.08
82	$C_3H_3N_2O^+$	0.07
108	$C_4H_2N_3O^+$	0.07
109	$C_4H_3N_3O^+$	0.21
110	$C_4H_4N_3O^+$	0.16
134	$C_5H_4N_5^+$,	0.09
135	$C_5H_5N_5^+$	0.06
151	$C_5H_5N_5O^+$	1.01
152	$C_5H_5N_5O^+$	0.07

single-charged molecular ions (the line $m/z = 135$ for adenine and the line $m/z = 151$ for guanine); (2) occurrence of a large number of lines with different intensity which correspond to the new-born ionic fragments; (3) the absence of lines of doubly charged molecular ions and of the dimer species.

To determine effective cross-sections for the formation of the ionic fragments one needs to make measurements of the absolute value of the total ionization effective cross-section of the adenine and guanine molecules. Results of such measurements are presented in Figures 3 and 4, where the absolute values of the total ionization effective cross-sections and their energy dependences (ionization functions) are given for the adenine and guanine molecules, respectively, in the energy interval from the threshold till 200 eV of the bombarding electrons energy. After the fast growing near the threshold, as follows from these figures, the ionization functions exhibit

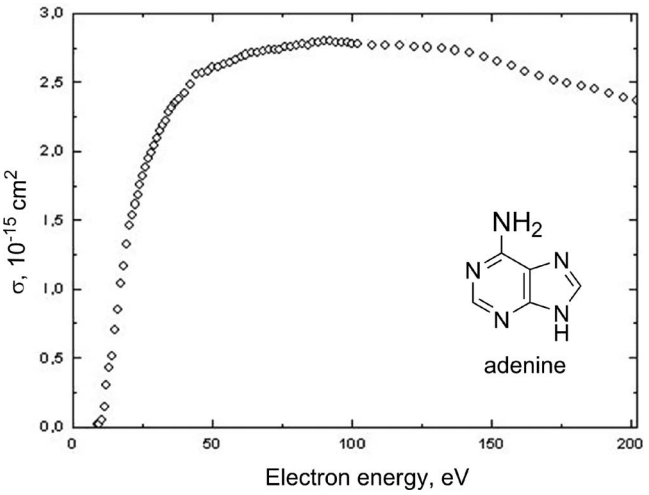

FIG. 3. The absolute cross section values for the formation of adenine positive ions.

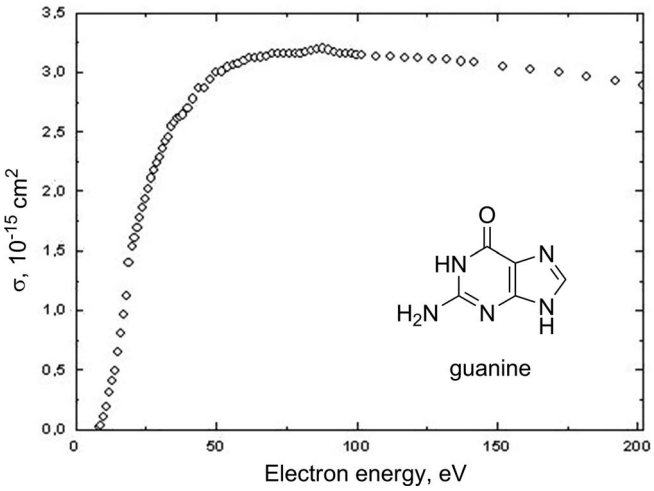

FIG. 4. The absolute cross section values for the formation of guanine positive ions.

gently slops with the weakly defined features and show wide maxima in the region 85–95 eV.

The maximum value of the total ionization cross-section of the adenine molecule is achieved at 90 eV of the electron beam energy and is equal to $(2.8 \pm 0.15) \times 10^{-15}$ cm^2 (Fig. 3). For guanine, the maximum value of the ionization cross-section is equal to $(3.2 \pm 0.15) \times 10^{-15}$ cm^2 and is observed at 88 eV (Fig. 4). The measured threshold of the positive molecular ion generation for adenine and guanine is equal to (8.8 ± 0.2) and (8.3 ± 0.2) eV, respectively. These values are in a reasonable agreement with the results of Refs. 20–28.

One should mention that the absolute values of the total ionization effective cross-section of the adenine and guanine molecules are quite close to each other. The higher cross-section for guanine correlates with its lower ionization potential. In Tables III and IV, the calculated adiabatic ionization potentials (IP) based on the complete geometry optimization of the molecules and ions by the DFT B3LYP method are presented together with various experimental results.

The Koopman's theorem in the AM1 approach predicts 8.77 and 8.40 eV for the adenine and guanine molecules, respectively, which agree pretty well with our IP experimental data. The DFT predication underestimates the ionization potentials (Tables III and IV); the DFT results based on the Koopman's theorem are even worse. They provide only qualitative agreement for the absolute values, but the relative values and difference between adenine and guanine ionization potentials are well reproduced in all quantum

TABLE III. Ionization potentials (IP) of adenine molecule.

IP, eV	Method	Source
8,8 ±0,2	Electronic impact	This work
8.3 ± 0.1	Electronic impact	Reference 22
8.48	PES	Reference 24
8.44 ± 0.03	Photoionization	Reference 21
7.98	B3LYP/6-31G (adiabatic)	This work
8.44	RHF/3-21G	Reference 28

TABLE IV. Ionization potentials (IP) of guanine molecule.

IP, eV	Method	Source
8.3±0.2	Electronic impact	This work
8.0 ± 0.2	Electronic impact	Reference 22
8.24 ± 0.03	Photoionization	Reference 21
8.1 ± 0.2	Electronic impact	Reference 20
7.52	B3LYP/6-31G (adiabatic)	This work
8.24	RHF/3-21G	Reference 28

chemical methods used. (0.48 eV in DFT and 0.5 eV in our electron impact measurements). The lower IP for guanine can be explained by the fact that the carbonyl group provides a particular non-bonding contribution into the highest occupied molecular orbital (HOMO) in guanine (see Fig. S1(b) of the supplementary material[45]). The long conjugation chain in the adenine molecule, N9–C4–C5–C6–N1, (see Fig. S1(a) of the supplementary material[45]) provides more stabilization of the adenine HOMO, while in the guanine HOMO this chain is cleaved at the C6 atom of carbonyl group, see Fig. S1(b) of the supplementary material.[45]

The measured ionization cross-sections have the meaning of the total cross-section, thus they include cross-section of generation of the starting molecular ions and of their fragments (the partial cross-sections). On the ionization curves (Figs. 3 and 4) one can see the features in the form of twists and bends, which can be interpreted as the processes of dissociative ionization and by generation of excited ions.

The obtained data on the total ionization cross-section of the adenine and guanine molecules and on their mass spectra permit us to determine the partial cross-sections of the most probable ion fragments formation at the 95 eV energy of the bombarding electrons (Tables I and II, where σ is the partial cross-section). The absolute values of the partial ionization cross-sections are determined by their normalization to the absolute values of the total ionization cross-section according to the following method.

It is obvious that the summarized current of the generated ions is equal to $i_\Sigma = i_1 + i_2 + \ldots + i_n$, where i_n is an ionic current of a particular fragment. From the other hand: $i_\Sigma = i_e n \sigma_\Sigma l$ and $i_n = i_e n \sigma_n l$, where i_e is a current of the bombarding electrons, n is a concentration of molecules in the region of beams crossing, l is the electrons path length in the molecular beam, σ_Σ and σ_n are the total and partial ionization cross-sections, respectively. From this analysis, it follows that $\sigma_n = \sigma_\Sigma i_n / i_\Sigma$. Accounting that the ionic current is proportional to the mass spectral peak intensity, we obtain the following partial cross-section: $\sigma_n = \sigma_\Sigma S_n / \sum S_i$, where S_n is the intensity of the nth peak; in denominator is the sum of all peaks intensity in the mass spectrum.

Analysis of Tables I and II indicates that formation of the adenine and guanine molecular ions are the predominant processes (cross-section of the order of 10^{-15} cm^2) (as well as for cytosine, thymin and uracil molecules),[4,8–11] which testify to the high-enough stability of the studied nucleobases with respect to electron impacts. This is a very important fact for such complicated species as adenine and guanine consisting of two heterocyclic rings. Many complicated molecules do not possess the stable molecular ions.[1–6]

TABLE V. The optimized bond length for the adenine molecule and cation-radical calculated by the AM1 and B3LYP/6-31G approaches (the corresponding bond length differences ΔR between cationic (M^+) and neutral (M) species are also presented).

	$C_5H_5N_5$ (M)		$C_5H_5N_5^+$ (M^+)		ΔR (M^+–M)	
Bond	AM1	DFT	AM1	DFT	AM1	DFT
N10–C6	1.368	1.355	1.340	1.328	− 0.028	− 0.027
C6–C5	1.437	1.411	1.461	1.429	0.024	0.018
C5–N7	1.402	1.400	1.356	1.356	− 0.046	− 0.044
N7–C8	1.342	1.326	1.391	1.365	0.049	0.039
C8–N9	1.413	1.393	1,380	1.364	− 0.033	− 0.029
N9–C4	1.399	1.384	1.422	1.395	0.023	0.011
C4–C5	1.459	1.404	1.503	1.433	0.044	0.029
C4–N3	1.368	1.350	1.327	1.317	− 0.041	− 0.033
N3–C2	1.353	1.351	1.401	1.400	0.048	0.049
C2–N1	1.360	1.355	1.329	1.327	− 0.031	− 0.028
N1–C6	1.376	1.360	1.402	1.379	0.026	0.019

To find the most probable scheme of fragmentation under the electron impact the results of quantum chemical calculations of the adenine and guanine molecules and of their cations by DFT and AM1 methods are analyzed (Tables V and VI). The standard numeration of atoms is presented in Fig. 5. The optimized bond lengths of the molecule and cation are compared. Those chemical bonds which are elongated and hence getting weaker upon ionization should indicate the most probable routes of fragmentation. We propose that the most probable cleavages have to be around those atomic positions in the ion, where the sums of two elongated chemical bond lengths changes are the largest ones upon ionization. Originally we have assumed that only two bonds can be cleaved simultaneously in the ion. Analysis of all possible dissociation routes has supported this assumption latter on.

1. Adenine

One can pay attention to those ionic fragments, which show the largest formation cross-sections. For adenine these are the following fragments: $C_4H_4N_4^+$, $C_3H_3N_3^+$, $C_2H_2N_2^+$,

TABLE VI. The optimized bond lengths for the guanine molecule and cation-radical calculated by the AM1 and B3LYP/6-31G approaches (the corresponding bond length differences ΔR between cationic (M^+) and neutral (M) species are also presented).

	$C_4H_5N_4O$ (M)		$C_4H_5N_4O^+$ (M^+)		ΔR (M^+–M)	
Bond	AM1	DFT	AM1	DFT	AM1	DFT
O11–C6	1.239	1.243	1.229	1.232	− 0.010	− 0.011
C6–C5	1.448	1.433	1.464	1.447	0.016	0.014
C5–N7	1.396	1.397	1.353	1.352	− 0.043	− 0.045
N7–C8	1.346	1.322	1.391	1.358	0.045	0.036
C8–N9	1.414	1.398	1.388	1.379	− 0.026	− 0.019
N9–C4	1.395	1.376	1.415	1.382	0.020	0.006
C4–N3	1.383	1.365	1.333	1.322	− 0.050	− 0.043
N3–C2	1.356	1.327	1.416	1.377	0.060	0.050
C2–N10	1.412	1.365	1.362	1.333	− 0.050	− 0.032
C2–N1	1.409	1.382	1.396	1.366	− 0.013	− 0.016
N1–C6	1.423	1.444	1.429	1.445	0.006	0.001

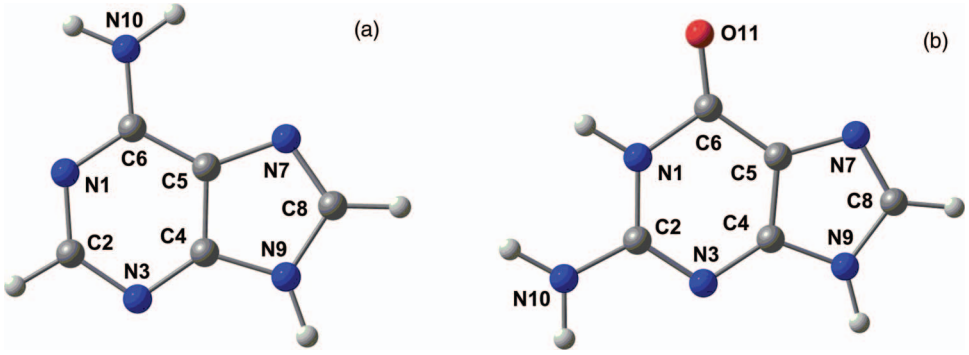

FIG. 5. The optimized structure and standard numeration of atoms for the adenine (a) and guanine (b) molecules.

$C_3H_2N_2^+$, $C_2HN_2^+$, CH_2N^+, CHN^+; for guanine—CHNO, CO^+, $CH_4N_2^+$, CH_2NO^+, $C_2H_2N_2^+$, $C_4H_5N_4^+$,$C_4H_3N_3O^+$, $C_4H_4N_3O^+$. The other fragments are characterized by significantly lower formation cross-sections $\sim (10^{-17}-10^{-18})$ cm^2.

As follows from Table V for molecular adenine ion, the most important two-bond dissociation routes are the following: 1. C6–C5, N1–C6; 2. C6–C5, N3–C2; 3. N7–C8, N9–C4; and 4. C6–N1, N3–C2. Probabilities of cleavage of these couples of chemical bonds are considered to be independent and the nascent fragments can be the source of the further dissociation. Thus, there are independent parallel-subsequent schemes of fragmentation (Fig. 6). Let us consider them in more details.

Route 1 (cleavage of the bonds C6–C5, N1–C6) and route 3 (cleavage of the bonds N7–C8, N9–C4) can be considered as almost equally probable. In those cases, the molecular ion $C_5H_5N_5^+$ loses the neutral fragment $C_4H_3N_4$ and produces the charged fragment CH_2N^+(m/z = 28). This ion is well seen in the mass spectrum (Fig. 1).

Route 2 (cleavage of the bonds C6–C5, N3–C2). Molecular ion $C_5H_5N_5^+$ loses the neutral fragment $C_2H_3N_2$ and produces the charged fragment $C_3H_2N_3^+$ (m/z = 80). The sum of these two bond-lengths changes upon ionization is one of the largest for the route 2 (0.067). The relatively low intensity of the line m/z = 80 (Fig. 1) can be explained by the high meta-stability of this ion. Our calculations show that the five-member cycle $C_3H_2N_3^+$ is unstable with respect to the cycle opening which finally leads to new fragmentation upon electron impact in the crossed beams region.

Route 4 (cleavage of the bonds N1–C6, N3–C2). This is the main route of the primary dissociation of the adenine cation $C_5H_5N_5^+$ since it is characterized by the largest sum of changes (0.068) of the two bond-lengths (N1–C6 and N3–C2). The simultaneous cleavage of these two bonds initiates the principal fragmentation chain, which explains occurrence of the large part of intense lines in the adenine mass spectrum:

$$C_5H_5N_5^+ \xrightarrow[]{-CHN} \underset{(m/z=108)}{C_4H_4N_4^+} \xrightarrow[]{-CHN} \underset{(m/z=81)}{C_3H_3N_3^+} \xrightarrow[]{-CHN} \underset{(m/z=54)}{C_2H_2N_2^+} \xrightarrow[]{-CHN} \underset{(m/z=27)}{CHN^+}. \quad (1)$$

This principal pathway involves the successive detachments of HCN or CNH groups (We shall not concentrate attention on the differences of these two isomers, though we can easily distinguish them in our theoretical simulations; we just refer to them as CHN for simplicity). The similar conclusions have been obtained by the authors of Refs. 18 and 19. The newborn "daughter" ions are not very stable and undergo further dissociation. In particular, the first charged fragment $C_4H_4N_4^+$ (m/z = 108) produced in the route 4 (Fig. 7(a)) undergoes one and two H-atom transfer producing the isomers (b) and (c) shown in Fig. 7. The ions (a) and (c) of Fig. 7 have been considered earlier.[19] Similar two isomers of the $C_4H_4N_4^+$ ion are denoted as (IIa) and (IIb) in Ref. 19, but their structure and charge distribution in our calculation are rather different from the canonic formulae proposed by S. Leach *et al.* (Fig. 8).[19]

The DFT-optimized structure of the primary $C_4H_4N_4^+$ ion (Fig. 7(a)) differs from the hypothetic structure (IIa) in Fig. 5 of Ref. 19, where the NH_2 group has a trans-orientation with respect to the C4=C5 double bond (Fig. 8). The late bond is not a double bond, but it is a very weak single bond (1.53 Å) in the DFT prediction (Fig. 7(a)); the NH_2 group is almost neutral (the N charge is −0.63, two H atoms bear +0.42 and +0.38), but the C6 atom bears the largest positive charge, +0.46. The structure of the ion is strongly polarized, including the hydrogen-bond fragment.

Our DFT calculation agrees with the hypothesis of Ref. 19 with respect to the spin density (ρ) concentration of the cation-radical $C_4H_4N_4^+$ mostly on atom C6 (ρ = 0.63): the rest of non-paired spin density is on the atom N3 (Fig. 7(a)). The intra-molecular H-bond of the primary $C_4H_4N_4^+$ ion (Fig. 7(a)) is an important new prediction of our DFT calculation. The cleavage of two bonds N1–C6 and N3–C2 upon ionization of adenine along route 4 (Fig. 6) will definitely lead to such species, which is more stable than the open form (IIa; Fig. 8) and is ready for H atom transfer. The intermediate species (Fig. 7(b)) is absent in the principal fragmentation scheme of Ref. 19, but it should definitely contribute to a large intensity of the signal (m/z = 108) in the adenine mass spectrum (Fig. 1), since it is 58.5 kcal mol^{-1} lower by energy than the primary $C_4H_4N_4^+$ fragment (Fig. 7(a)). A high exothermicity of the H atom transfer (a) → (b) leads to creation of vibrationally excited ion $C_4H_4N_4^+$ (Fig. 7(b)), which can dissociate along C5–C6 chemical bond. The loss of the CNH particle from the

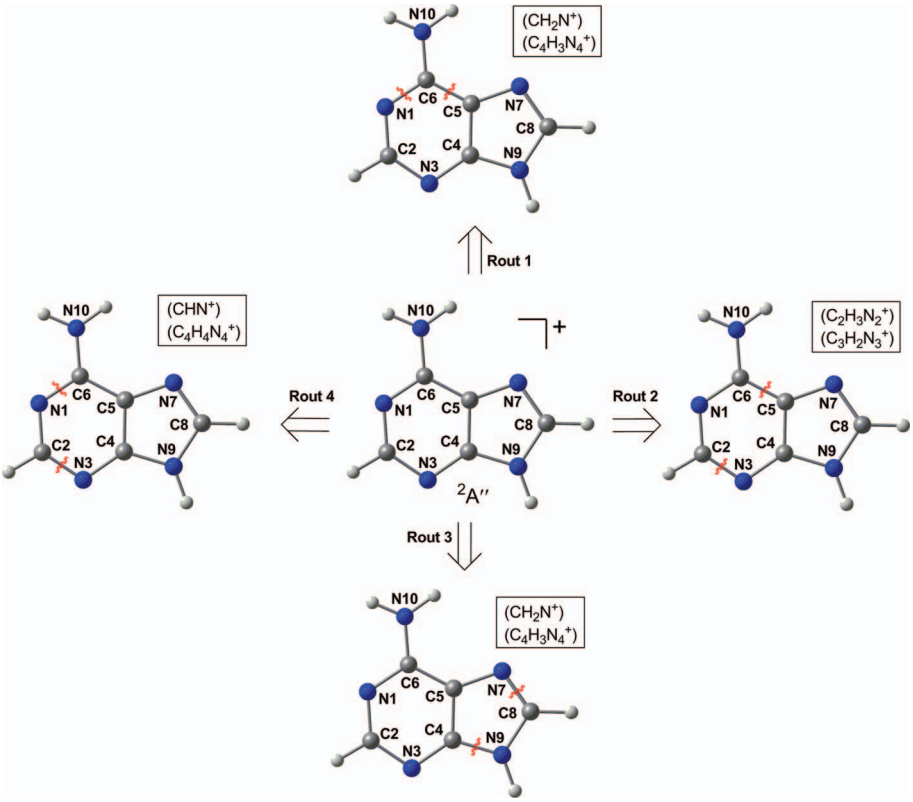

FIG. 6. The most probable routes of the adenine cation-radical fragmentation.

intermediate species (Fig. 7(b)) will lead to thermally non-stable ion $C_3H_3N_3^+$ (Fig. 7(d)), (m/z = 81), which further dissociate to $C_2H_2N_2^+$ (m/z = 54) loosing again the CNH particle.

The radical-cation in Fig. 7(d) (m/z = 81) is similar to the intermediate (IIIa) of Ref. 19; its largest spin density (ρ) is predicted for the atom C5 (ρ = 0.65) in a qualitative agreement with the hypothesis,[19] but other structural peculiarities

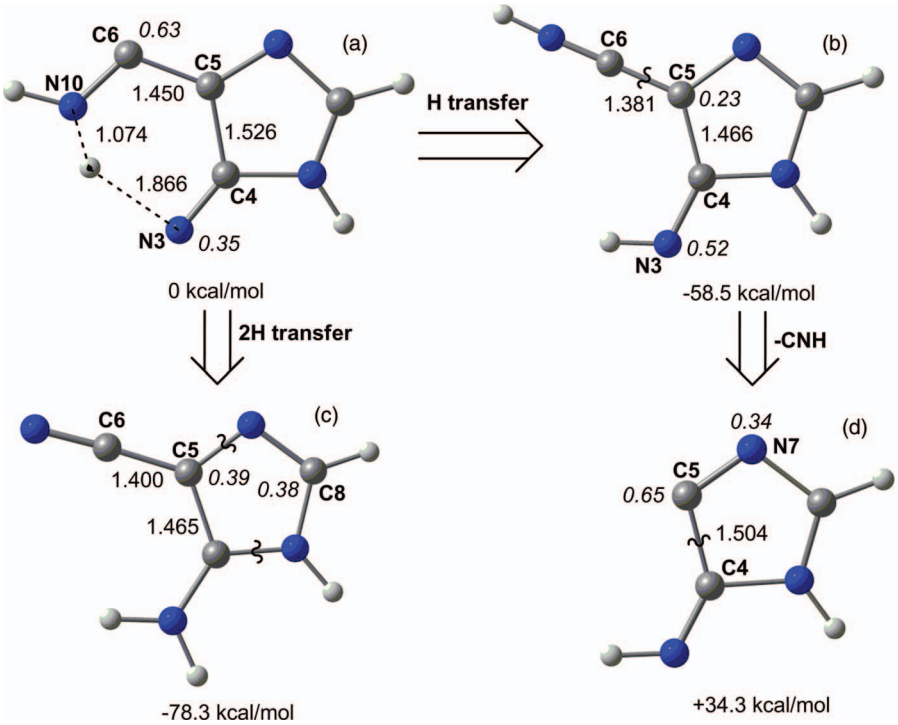

FIG. 7. The results of DFT/B3LYP/6-31G calculations for isomerisation and fragmentation of the intermediate $C_4H_4N_4^+$ cation-radical.

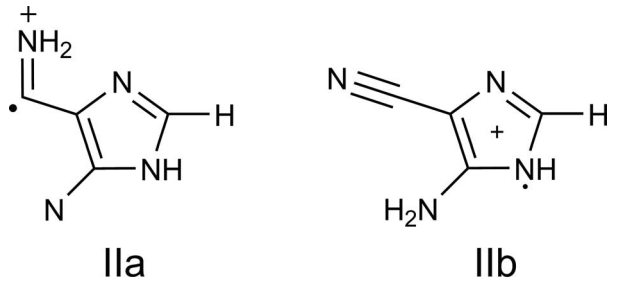

FIG. 8. Hypothetic structures of the $C_4H_4N_4^+$ cation-radical, proposed in Ref. 19.

are very different: the C4−C5 chemical bond is very weak (1.504 Å) and cannot be a double bond as it is shown in Fig. 5 of Ref. 19. According to DFT calculation, the short bonds are C5–N7 and C8–N9, thus being considered as double bonds in the ion $C_3H_3N_3^+$ (Fig. 7(d)). The cleavage of two other bonds C4–C5 and C4–N9 (1.47 Å) which are rather weak is the most probable dissociation process of the thermally non-stable ion (Fig. 7(d)). This leads to fragmentation into CNH molecule and the $C_2H_2N_2^+$ ion ($m/z = 54$) as presented in Eq. (1).

In Ref. 19, an additional step in the form of 1,3,5-triazine ion ($m/z = 81$) is considered. We need to exclude this (IIIb) step in Fig. 5 of Ref. 19 by the following reasons: (a) our DFT calculation predicts a symmetric C_{2v} structure of such ion with all almost equal C–N bond lengths (about 1.34–1.35 Å); this is the σ-radical being stable with respect to the HCN fragmentation; (b) the triazine ion ($m/z = 81$) is more stable by 23 kcal mol^{-1} than its isomer in Fig. 7(d) and cannot be involved as an intermediate step in the fragmentation cascade, Eq. (1). Though the triazine ion ($m/z = 81$) can be a deadlock product in the adenine mass spectrum (Fig. 1) explaining a relatively large intensity of the line ($m/z = 81$).

The product of two H atoms transfer (Fig. 7(c)) is the most stable among all $C_4H_4N_4^+$ ions ($m/z = 108$). This is the π-radical with spin distribution in the cycle and in the amino-group. In a complete contrast to the hypothetic structure IIb in Fig. 8, this π-radical has a negligible spin density at N9 atom and the most weak chemical bond C4–C5 (1.465 Å). The DFT calculations show that its rupture will lead to a linear fragment N10=C6–C5=N7–CH with a positive charge concentration, followed by a cleavage of the weak C8–N9 chemical bond. The rupture of this bond can be initiated by electron impact since it is much easier in the electric field of the approaching electron. Such fragmentation process leads to the NH_2CNH species and the $C_3HN_2^+$ ion ($m/z = 65$) formation, the late being indicated in the spectrum (Fig. 1). The cleavage of the C8–N9 chemical bond can be accompanied by a simultaneous H atom transfer from the terminal N9 atom to the CH group. Thus, the NH_2CN species and the $C_3H_2N_2^+$ ion ($m/z = 66$) can be formed. Such fragmentation scenario of the $C_4H_4N_4^+$ ions shown in Fig. 7(c) and predicted by quantum chemical calculations is in a good agreement with the observed mass spectrum (Fig. 1).

Transition of two hydrogen atoms from N10 to N1 provides a very exothermic process (Fig. 7), but we cannot find the transition state and activation energy of this reaction. We cannot exclude the two-stage process (a) → (b) → (c) in Fig. 7(a) and also the concerted reaction (a) → (c). Both these reactions are highly exothermic according to our DFT calculations with the reaction heat of 58 and 78 kcal mol^{-1}, respectively.

From our calculations we can explain the other possible dissociation processes. In particular, the $C_4H_4N_4^+$ ions ($m/z = 108$) can loss one or two H atoms providing 107 and 106 signals in the mass spectrum (Fig. 1). When the ion $C_3H_3N_3^+$ (Fig. 7(d)) loses hydrogen we get a biradical: the ion $C_3H_2N_3^+$ ($m/z = 80$) with the N–H bond lost at the N9 atom. The singlet and triplet states of this biradical are almost degenerate (non-paired spins are localized at N3 and C5 atoms). Ruptures of other N–H bond and of the C8–H bond also lead to biradicals, but with much higher energy. Since the singlet and triplet states are equally probable in the $C_3H_2N_3^+$ ion, a relative intensity of the signal $m/z = 80$ is significant (Fig. 1). Decay of the fragment $C_2H_2N_2^+$ ($m/z = 54$) with a subsequent loss of hydrogen atoms produces the $C_2H_1N_2^+$ ($m/z = 53$) and $C_2N_2^+$ ($m/z = 52$) ions. If a fragment $C_4H_4N_4^+$ (Fig. 7(c)) loses the CH_2N group, as considered above, the $C_3H_2N_2^+$ ion ($m/z = 66$) is formed. The late can lose hydrogen atoms subsequently and produce $C_3HN_2^+$ ($m/z = 65$) and $C_3N_2^+$ ($m/z = 64$) fragments. All corresponding lines are present in the adenine mass spectrum. In Ref. 19, the occurrence of $C_4H_3N_4^+$ ($m/z = 107$), $C_3H_2N_3^+$ ($m/z = 80$), $C_3H_2N_2^+$ ($m/z = 66$), and $C_3HN_2^+$ ($m/z = 65$) ions is explained in a rather different way and the line $m/z = 64$ is absent in the photoionization spectrum of adenine.[19]

The decomposition of the ion in Fig. 7(c) can include also the alternative fragmentation to NH_2CN^+ and the neutral $C_3H_3N_2$ species. Dissociation to the NH_2CNH^+ ion species and the C_3HN_2 radical is also possible. Thus the ions with the $m/z = 43$, 42, and 41 signals occur. An attempt to explain the occurrence of the late ions by the three bond rupture: N1–C6; N3–C2; and N10–C6 can be rejected by DFT calculation since the bond N10–C6 becomes stronger upon ionization (Table I). All other three-bond cleavages, which could lead to the observed ions are impossible, since they include rupture of those chemical bonds which are getting stronger upon ionization. This finding additionally supports a conclusion about non-importance of simultaneous three-bond cleavages.

2. Guanine

Guanine has the lowest oxidation potential among nucleic acid bases; thus, it plays a crucial role in oxidative DNA damage. The presence of the C=O group in guanine provides essentially different mass spectrum and fragmentation schemes from those of the adenine ones. In particular, there is no main fragmentation chain for guanine, which could explain occurrence of a large part of intense lines in its mass spectrum like the Eq. (1) provides in the adenine case. The obtained spectrum of guanine (Fig. 2) in general features is similar to the spectra, presented in Refs. 18–21. The difference concerns the intensity distribution and the number of lines. The possible reasons for such distinctions have been mentioned above.

The most intense line corresponds to the guanine molecular ion. Like in the case of adenine, fragmentation of

molecular ion requires simultaneous cleavage of two chemical bonds. As follows from Table VI, we can consider such couples of bonds: 1. C6–C5, C6–N1; 2. C6–C5, N3–C2; 3. C6–C5, C2–N1; 4. N3–C2, C6–N1; 5. C2–N1, N3–C2; and 6. N7–C8, N9–C4. Probabilities of these bonds cleavages can be considered as being independent ones and the new-born fragments can be the sources of further dissociation. Thus the following fragmentation schemes should be analyzed.

Route 1 (cleavage of the bonds C6–C5, N1–C6). Molecular ion $C_5H_5N_5O^+$ loses the neutral fragment $C_4H_5N_5$ and produces the charged species CO^+ ($m/z = 28$). The line 28 is the third line in terms of intensity (Fig. 2). An additional contribution to this line intensity provides the charged fragment CH_2N^+ produced by the routes 6 and 5, though the late contribution cannot be significant, because of the C2–N1 bond stabilization upon the primary ionization process (the root 6 is more preferable, Table VI). In turn, the fragment CH_2N^+ loses the hydrogen atom and transforms into CHN^+ ion ($m/z = 27$), which is also present in Fig. 2. One should say that the line 28 is absent in the mass spectra presented in Refs. 19–21, but it is well seen in the spectrum of Ref. 18, though Rice *et al.*[18,27] suppose that decarbonylation is not a significant decomposition reaction for the guanine ion. The presence of the CHN^+ ion can be considered on the backgrounds presented in Refs. 29 and 30.

It is important that identification of the line 28 with the CO^+ fragment is confirmed by indirect experimental corroboration. Thus, in Ref. 9, a photoemissive uracil spectrum initiated by electron impact has been detected and analyzed. The uracil molecule similar to guanine possesses a carbonyl group. It was shown[9] that several intense lines in the uracil luminescence spectrum are well identified with molecular rovibronic bands of the CO^+ ion (a progression of the first negative system $B^2\Sigma^+ \rightarrow X^2\Sigma^+$) and of the CO molecule. Calculations indicate that the root 1 is accompanied by weakening of both C6–C5 and N1–C6 chemical bonds upon ionization and also by concentration of positive charge on the C=O fragment in the ion. These results are obtained in both DFT and AM1 methods (Table VI); they agree also with the B3LYP/6-31+G** results.[31]

Route 3 (cleavage of the bonds C6–C5, N1–C2). Molecular ion $C_5H_5N_5O^+$ loses the neutral fragment $C_4H_4N_4$ and produces the charged species $CHNO^+$ ($m/z = 43$) with the most intense line behind the main molecular ion (Fig. 2). This route cannot be very efficient since the bond N1–C2 is shortening (enhanced) upon ionization (Table VI). Moreover, detailed calculation of the step-wise elimination of the $CHNO^+$ ion predicts this process to be impossible in contrast to the neutral HN=C=O species production (see Fig. S2 of the supplementary material).[45]

At the same time the route 4 (N3–C2, C6–N1) leads to the same $m/z = 43$ signal with the loss of the $CN_2H_3^+$ ion. Rice *et al.*[18,27] consider just that ion; attachment of the H atom by this ion in the beams crossing region can explain the assignment of the $m/z = 44$ line to the cyanamide ($CN_2H_4^+$) cation. The route 4 is quite probable since it includes the large lengthening of the N3–C2 chemical bond upon ionization with a simultaneous relaxation of the second link (Table VI).

Analysis of mass spectrum requires one more additional route 7 (cleavage of the bonds C4–N3, N1–C2) when the molecular ion $C_5H_5N_5O^+$ loses the neutral fragment CH_2N_2 and produces the charged species $C_4H_3N_3O^+$ ($m/z = 109$). This route 7 is rather difficult; it requires cleavage of two bonds, which are getting stronger upon ionization. Geometry of the nascent ion $C_4H_3N_3O^+$ is not changed much during fragmentation (see Fig. S3 of the supplementary material)[45], but the process requires additional energy of 156 kcal mol^{-1} according to our calculation.

Electronic-vibrational excitation of the ion upon collision and vibronic relaxation depend on equilibrium position displacements for anharmonic oscillators. Those chemical bonds, which experience elongation upon ionization can accept and concentrate more collisional energy because of the higher Franck-Condone factors (like in the usual vibronic progressions in absorption spectra). The plane wave of colliding electron interacts with molecular (ionic) wave function in a similar manner like a mass-less photon of electromagnetic wave interacts with electronic shell in terms of vibronic excitation. Thus, we assume that the largest elongation of two chemical bonds upon ionization would concentrate more energy and corresponding fragmentation should dominate in the mass spectrum. The above example with the 109 mass represents some exclusion from this simple semi-empirical rule and requires additional comments.

All possible orientations of rotating molecule with respect to the electron beam direction are realized before collision. In our analysis of possible fragmentation routes we use a simple quasi-classical assumption that colliding electron does not change (most probably) its trajectory during the primary collision and cuts the polyatomic molecule along a straight line. With such primitive idea in mind we consider two-bond scission routes in the nucleobases. Fortunately, this intuitive approach helps us to rationalize the observed mass spectra with account of predicted structural changes upon ionization. The route 7 satisfies the linear trajectory idea, but contradicts the vibronic relaxation and bond strengths redistribution concept.

The ion $C_4H_3N_3O^+$ ($m/z = 109$) (see Fig. S3 of the supplementary material)[45] is relatively stable with respect to further dissociation. All vibrational frequencies are real and the lowest one is equal to 49.5 cm^{-1}; this indicates a hard skeleton of the $C_4H_3N_3O^+$ ion (see Fig. S3 of the supplementary material).[45] It is separated from further fragmentation by large activation barriers. For example, the C5–C6 bond cleavage has activation energy of 51 kcal mol^{-1}. The single-occupied MO in this radical-cation (see Fig. S3 of the supplementary material)[45] represents the sp^2 orbital at the N1 atom with small contribution from the O11 lone pair. Thus, this radical is more similar to a physically stable molecule with a typical five-member ring.

The loss of ammonia (151–17 = 134) and amino group (135) from the primary ion (151) provides the moderate signals in guanine mass spectrum (Fig. 2). The loss of NH_3 frequently happens for the dissociation of guanine related ions.[31] The process has started with the pyrimidine ring opening by the cleavage of the C6–N1 bond with simultaneous multiple hydrogen transfer. Then the N1 and N10 atoms have some

chance to chip off (N1 accounts just for 3%–4% of N10 for the loss of ammonia). It was mentioned[31] that the loss of NH_3 from guanine cation is very similar to that from protonated guanine. According to our calculations the guanine radical-cation and protonated guanine at the N10 atom have very similar heat of formation (192 and 188 kcal mol^{-1}, respectively) and the form of the HOMO π–orbital. The only difference concerns the fact that the p_π AO on N10 is fully ionized (+0.92) in the protonated ion and is only partly ionized (+0.32) in the guanine radical-cation.

Cheng *et al.*[31] have studied the gas-phase guanine cation generated by electrospray ionization (ESI) and its dissociation induced by collisions. The five dissociation mechanisms have been calculated[31] for the ESI-induced guanine cation including elimination of NH_3, HCN, H_2NCN, HNCO, and N=C=NH and few possible isomerizations.

According to DFT calculation,[31] the loss of ammonia includes multiple hydrogen transfers with subsequent opening of the pyrimidine ring through the N1–C6 bond rupture. The corresponding transition state (TS) has the activation energy of 95.3 kcal mol^{-1}, which is higher than that for other fragmentation processes. This explains the relatively weak line $m/z = 134$ in the spectrum (Fig. 2) in spite of the rather simple mode of the pyrimidine ring cleavage and the fact that the rupture of the N1–C6 bond is slightly facilitated by ionization (Table VI). The amino group loss provides a low intensity line ($m/z = 135$) because the C2–N10 bond is getting shorter upon ionization (Table VI); thus, the energy concentration on this oscillator is less probable and the cleavage is hindered.

The loss of the HCN molecule (27 amu) could lead to the ion (151–27 = 124). Such mass is absent in the spectrum (Fig. 2). Potential energy surface for such fragmentation of the primary ion includes TS with very high activation energy (115 kcal mol^{-1})[31] and the large entropy change, which explains the absence of the signal in our mass spectrum.

An attempt to explain the appearance of the $CHNO^+$ ion ($m/z = 43$) (scrutinize the route 3) through the cascade of H atoms transfer and the rupture of the N1–C2 bond with a subsequent cleavage of the C5–C6 chemical bond (in accordance with the model of Ref. 31) has failed. The TS and the product of such route are shown in Fig. S2 of the supplementary material.[45] Instead of the ion, we get a neutral species HN=C = O with a quasi-linear NCO chain. According to our calculation, ionization potential of this stable molecule is equal to 10.2 eV, while the residual fragment (the rest $C_4H_4N_4$ species, see Fig. S2(b) of the supplementary material[45]) has much lower ionization energy (7.3 eV); thus we cannot explain the ($m/z = 43$) line in the mass spectrum by occurrence of the ion $CHNO^+$ along the route 3. In the transition state (see Fig. S2(a) of the supplementary material[45]) almost the whole charge and spin density are concentrated on the $C_4H_4N_4^+$ ion ($m/z = 108$). An ion of the same mass is observed in mass spectra of both purine nucleobases, but in the adenine spectrum the line 108 has much higher intensity (Fig. 1). A complicated multi-step route of this fragmentation in the guanine ion explains this difference. We have to remind that the structure of the $C_4H_4N_4^+$ ion from adenine (Fig. 7) and guanine precursors (see Fig. S2 of the supplementary material[45]) are completely different.

For occurrence of the ions with the $m/z = 54$, 53 signals we need to assume a stepwise process of the C5–C6 bond cleavage which becomes weak upon ionization (Table VI) with subsequent rupture of the C5–C4 and C4–N9 bonds (all bonds are stretched during ionization). This leads to the neutral $C_3H_3N_3O$ species and the charge fragment $C_2H_2N_2^+$ ($m/z = 54$); the loss of hydrogen from the late ion generates a new signal $m/z = 53$. Our DFT calculations support such scheme according to spin distribution and total energy analysis for the neutral and ionized fragments. The ion $C_2H_2N_2^+$ ($m/z = 54$) is shown in Fig. S4 of the supplementary material;[45] its charge is almost equally distributed among all atoms (excepting N7 which bears small negative charge −0.2). The structure of the ion C=N–CH–NH includes the NCN angle equal to 119.8° with a typical sp^2 hybridization at the C8 atom, while the terminal CNC and CNH groups are close to be linear; the whole spin of this σ-radical cation is concentrated at the N9 atom. The neutral $C_2H_2N_2$ species have a bent CNH group with the angle 117.9°; thus, the N9 atom changes the sp^2 hybridization to sp hybridization upon transition from the neutral molecule to the ion. This structural change provides additional stabilization of the $C_2H_2N_2^+$ ion, which is well seen in the guanine mass spectrum (Fig. 2).

The above schemes of fragmentation are rather different from those presented in Refs. 18, 19, and 31. Our schemes are based on numerous DFT calculations of various tentative intermediates and fragments; they seem to be the most probable, but we cannot exclude alternative explanations of mass spectra of the adenine and guanine molecules induced by electron impact.

B. Negative ions

The negative ionization cross-sections of the adenine and guanine molecules are presented in Figs. 9 and 10. The intrinsic interaction of low-energy electrons with gas phase adenine and guanine have been studied extensively during last decade.[31–37] Huber *et al.*[11] have shown that fragmentation of

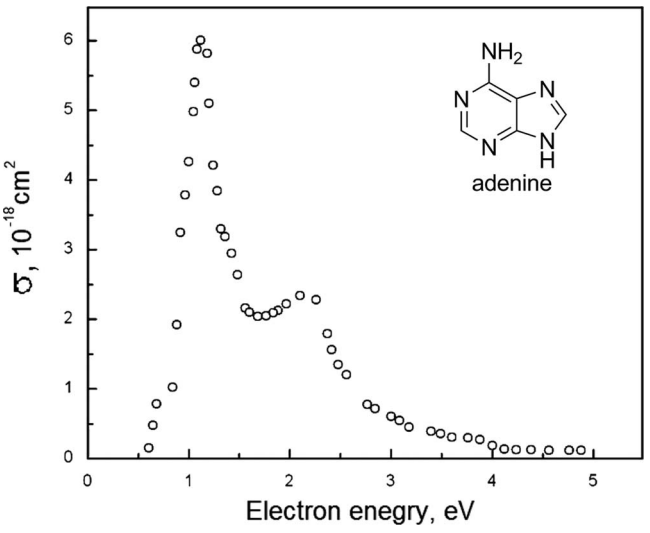

FIG. 9. The absolute cross section values for the formation of adenine negative ions.

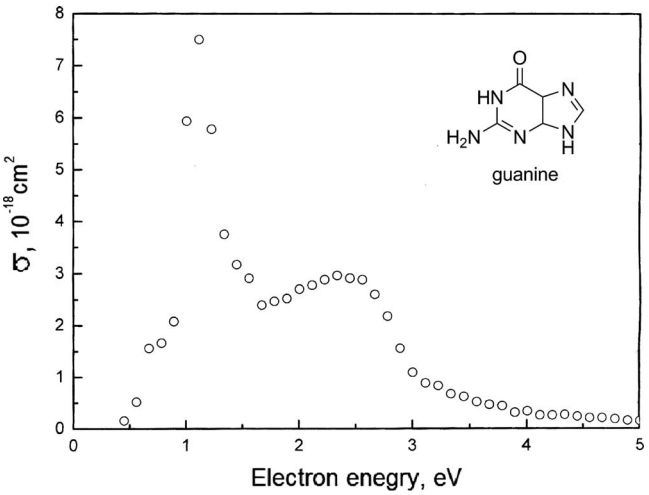

FIG. 10. The absolute cross section values for the formation of guanine negative ions.

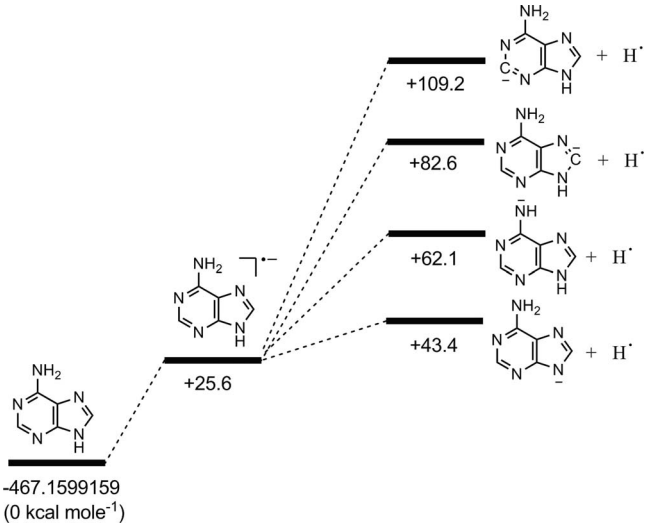

FIG. 11. The energetic diagram for electron attachment to the adenine molecule with the subsequent C–H/N–H homolysis of the adenine anion-radical.

adenine is restricted to a few negatively charged species. In contrast to that, guanine decomposes into a variety of negatively charged fragments via a number of complex unimolecular reactions upon collisions with electrons in the entire energy range of 0–10 eV.[34,35] The thermodynamic threshold ΔH^0 for a simple bond dissociation process in a molecule MX initiated by an electron impact, $e^- + MX \rightarrow M + X^-$, can be expressed as: $\Delta H_0(X^-) = D(M{-}X){-}EA(X)$, where $\Delta H_0(X^-)$ is the threshold energy for the observation of the X^- species, D(M–X) is the bond dissociation energy and EA(X) is the electron affinity of the corresponding radical.

1. Adenine

Our crossed beam experiment show that in contrast to positive ions, the formation of negative adenine ions occurs in a very narrow energy region of the bombarding electrons (Fig. 9), which indicates the resonance character of the process. The maximum value of the negative ionization cross-section of the adenine molecule is achieved at 1.1 eV of the electron beam energy and is equal to $(6.0 \pm 1.2) \times 10^{-18}$ cm^2 (Fig. 9). This cross-section is the total one and includes formation of negative ions of the former molecule and of its fragments.

By an electron capture, the adenine molecule becomes a negative ion in an excited state. This anion is unstable and strives for avoiding of the extra energy. According to the energy conservation law, this is possible through dissociation of the molecular ion. One of the fragments would be a negative ion, the other—atomic hydrogen. The DFT calculated bond lengths in the negative molecular ion indicate a possible place of the bond rupture. We also have calculated by DFT method the energy diagram for the adenine molecule, its anion-radical and the possible routs of the anion dissociation (Fig. 10).

One can see from Fig. 11 that an electron attachment to the adenine molecule requires the energy increase of 25.6 kcal mol^{-1} (this corresponds to a negative electron affinity (EA) equal to −1.11 eV being close to other experimental data −1.0 eV).[32,33] It is interesting to note that EA calculated by Koopmans theorem[38,39] (EA $= -\varepsilon_{LUMO}$) in the framework of PM3 method is positive (0.45 eV) as well as the adiabatic EA value. Thus, the semi-empirical PM3 method is not reliable for this anion. The Koopmans theorem in DFT approach also predicts a positive EA value (0.3 eV) which contradicts to the direct adiabatic calculation with a complete geometry optimization of the neutral and anionic forms of adenine. (It is well known that DFT method does not provide reliable MO energies;[38] therefore the Koopmans theorem is not reliable for the EA measurements of adenine and guanine molecules, Tables III and IV).

We suppose that the weak cross-section features below 1 eV in Fig. 9 correspond to thermally activated adenine molecules in the beam. The thermally excited N-H vibrations in the imidazole ring (3340 cm^{-1}) just satisfy to the small left shift from the main peak of about 0.4 eV in Fig. 9. Stretchings of the C–N bonds (C2–N3 and C8–N7) are also very important during electron attachment, since their force fields are strongly relaxed upon anion formation (see Table V). Their thermal excitation also leads to additional cross-section of the negative ionization. These vibrations are the most important for the anion formation cross-section since they afford to facilitate an electron attachment by the corresponding nuclear displacements through the Franck-Condone factor increase and stabilization of the anion.

The anion-radical produced by the resonant electron attachment in the ground state is quite stable because of significant delocalization of the non-paired π–electron (see Fig. S5(a) of the supplementary material);[45] that is why the spin density in the anion-radical is delocalized and it is impossible to specify some particular radical center. By these reasons, all possible dissociations of the ion are endothermic processes. As follows from our DFT calculations (Fig. 11) the most probable result of an electron attachment upon low-energy beam impact could be a generation of the closed-shell singlet ground state anion produced by separation of hydrogen atom from the N9 nitrogen of imidazole ring. The first shoulder at 1.5 eV in Fig. 9 indicating a small increase of

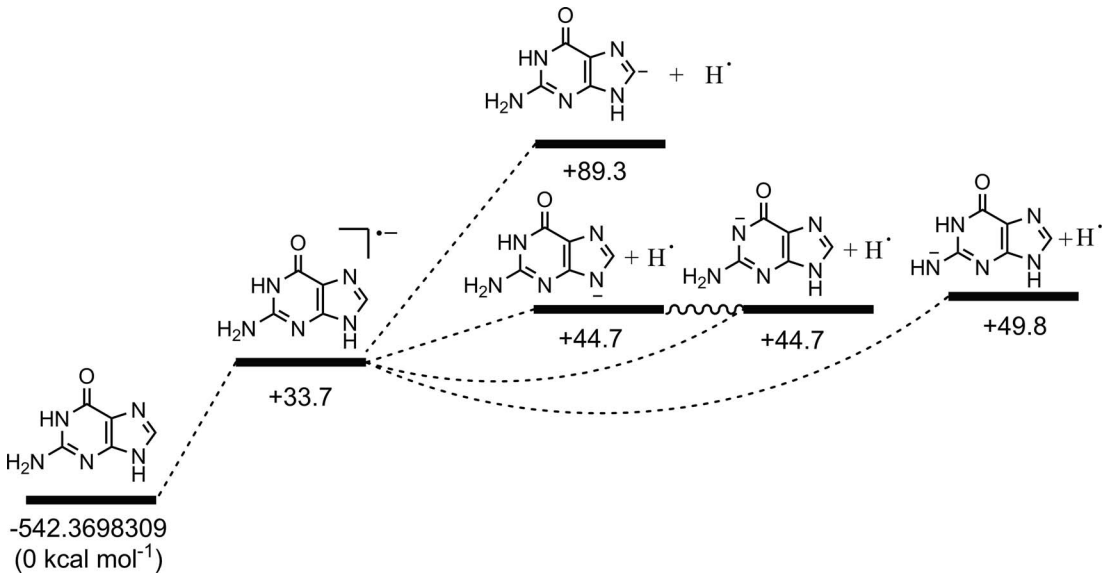

FIG. 12. The energetic diagram for the electron attachment to the guanine molecule with the subsequent C–H/N–H homolysis of the guanine anion-radical.

the negative ionization cross-section of the adenine molecule, probably, is connected with the N9–H bond rupture. A strong peak at 2.2 eV in Fig. 9, one can connect with the amino-group N–H bond cleavage. In a similar manner, the weak features at 3.8 and 4.7 eV in the cross-section energy dependence (Fig. 9) could be assigned to the corresponding C–H bonds dissociations, which need more energy (Fig. 10). The agreement with calculated energy will be higher if the zero-point vibrational correction would be taken into account. Thus, the dissociative electron attachment (DEA) to gas phase adenine molecule in the beam can be qualitatively interpreted on the ground of our DFT calculations.

In the study of Abdoul-Carime *et al.*,[36] the negative ions formed via electron-molecule collisions were extracted from the reaction volume by a small electric field towards a quadrupole mass analyzer, and are detected by single pulse counting techniques; thus, a particular anion yield was recorded. In the range below 5 eV, only yield of the $(A–H)^-$ type anions (134 amu) was obtained. Two peaks at the ion-yield spectrum for these anions with the mass 134 amu in Ref. 36 correspond to the features at 1.18 and 2.17 eV in our Fig. 9. Ion efficiency curve for dehydrogenation of adenine anion via DEA, obtained by Huber *et al.*[11] also coincides well with our data (Fig. 9). Thus, our DFT interpretation (Fig. 11) of the DEA cross-section in Fig. 9 agrees well with results of Refs. 11 and 36. Other processes, besides dehydrogenation, occur around 6–7 eV,[36] which are not relevant to our study.

2. Guanine

The dissociative electron attachment to guanine is less clear. In a striking contrast to other nucleobases, guanine behaves very different upon low-energy electron collisions.[31–37] This means that dehydrogenation is comparatively weak in guanine anion, while various further decomposition reactions are observed from the low energy π^* precursor ions. The anion-radical produced by the resonant electron attachment is also characterized by significant delocalization of the non-paired π–electron, see Fig. S5(b) of the supplementary material.[45] These reactions lead to the fragment ions of the form $(G–O/NH_2)^-$, O^-/NH_2^-, $(G–HOCN)^-$, OCN^-, CN^- indicative of single bond cleavages, but also more complex unimolecular decompositions associated with the excision of cyano units from the cyclic structure.[36] The DEA cross-section for guanine dehydrogenation at the peak maximum in the measurements of Abdoul-Carime *et al.*[36] results to be 5×10^{-18} cm^2, which is in a good agreement with our data (7.8×10^{-18} cm^2).

Xie and Cao[35] presented potential energy surface profiles along various N–H and C–H bond dissociations in the anionic guanine obtained by DFT calculations. Our calculations (Fig. 12) are in general agreement with the results of Xie and Cao.[35] First, one can stress that dehydrogenation of guanine anion needs much higher energy than that of adenine anion (Fig. 10). Furthermore, the scissions of various N–H and C–H bonds are almost equally endothermic. This is in agreement with the diffuse second peak in ionization cross-section for guanine in comparison with that of adenine.

Burrows *et al.*[33,34] outlined a common range of attachment energies into the lowest orbitals observed in all nucleobases. Evidence for nuclear motion during the lifetimes of the anions is found in all the compounds except adenine.[33] This demonstrates that electron injection into the lowest unoccupied π^* orbitals of guanine produces strongly excited vibrational modes.[30] Calculations show that LUMO in guanine is antibonding with respect to C=O, N1–C2, C2–N3, C4–C5, C4–N9, and N7–C8 chemical bonds (see Fig. S5(b) of the supplementary material);[45] this means that electron attachment produces a great change in the force field of the species with respect to the neutral molecule.

Wiley *et al.*[37] have presented measurements of reversible reduction potentials of the nucleo-bases in solution, from which they have extracted gas-phase adiabatic electron affinities (EA) through calibration by comparison with other molecules for which both quantities are known. Their

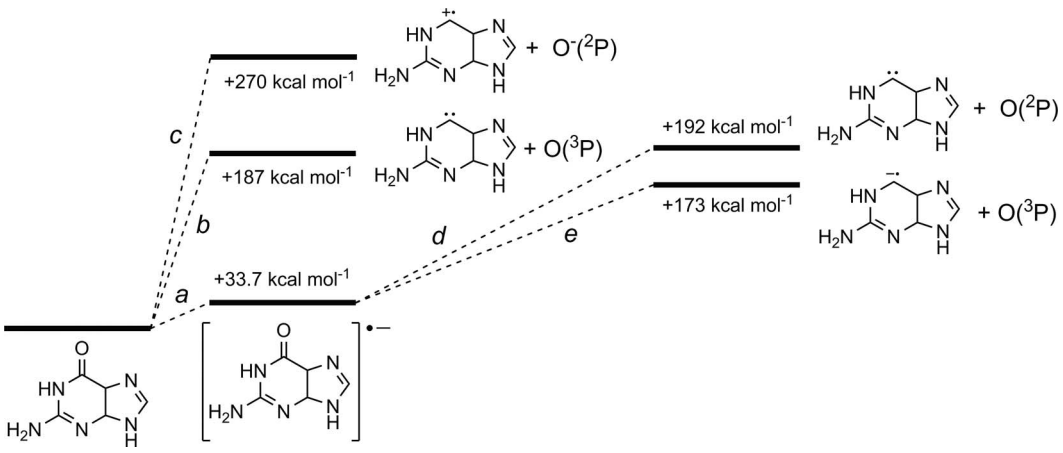

FIG. 13. Possible routs of oxygen elimination from the neutral guanine molecule (b, c) and from the guanine anion (d, e).

electron affinities for adenine and guanine are equal to +0.95 and +1.51 eV, respectively. These values are in a good agreement with our results of adiabatic DFT calculations (−1.11 and −1.46 eV, respectively). The only difference concerns the sign of electron affinity definition. We want to stress that an electron attachment to this molecules is an endothermic process (Figs. 11 and 12), thus EA is negative. In terms of Kopmans theorem, EA = $-\varepsilon_{\mathrm{LUMO}}$, thus the exothermic attachment corresponds to a positive EA value. Aflatooni *et al.*[33] have mentioned that the energies required to add an electron to the four DNA bases under the conditions of electron scattering are *positive*. Their explanation is based on the idea that the anion states at the equilibrium geometry of the neutral molecule are *temporary*, that is, unstable against electron auto-detachment, and make the anion appearance as "resonance" peaks in electron scattering cross-sections.[33] Stated more properly, the vertical attachment energies are all >0, or in a more familiar language, the vertical EA < 0.[33] Our DFT calculations indicate that adiabatic EA are also negative for adenine (Fig. 11) and guanine (Fig. 12), being in agreement with our interpretation of the cross-section curves (Figs. 9 and 10).

A comparative study of the low-energy electrons interaction with adenine and guanine should be interesting from a structural point of view. Our results are in agreement with the recent experimental observations showing that the purine nucleobases, adenine, and guanine can be decomposed by electrons of very low energy.[31–35] The decomposition of adenine (A) produces main fragments (A-H)−(134 amu) and (A-HCN)−(108 amu), CN−(26 amu) (both at high electron energy) where the dehydrogenation processes (A-H) represents about 95% of the total yield.[36] In contrast, the fragmentation of guanine upon dissociative electron attachment provides much more various anionic fragments and the dehydrogenation channel is a minor one; it stands for about 5% of the total fragment yield.[33] The decomposition of guanine by low-energy electrons generates more different anionic fragments attributed to (G–H)− (150 amu), (G–NH_2)− (135 amu), (G–OCNH)− (108 amu), OCN− (42 amu), CN− (26 amu), and (O and/or NH_2)− (16 amu). All of them occur below 5 eV.[36] We decided to analyze an occurrence of the late ions with the 16 amu mass, since they produce a small peak at about 2 eV in the ion-yield spectrum measured by Abdoul-Carime *et al.*[36] A detailed interpretation of such low-energy electron collisions with the oxygen elimination from guanine molecules will help us to assign a wide feature around 2 eV in Fig. 10. We have calculated with the DFT geometry optimization few different products of the oxygen elimination from the neutral guanine molecule and from its anion (Fig. 13).

The double C=O bond is rather strong and its homolytic cleavage from the neutral guanine molecule requires high energy (187 kcal mol^{-1}). This cleavage leads to two triplet species (the total spin is zero and the process is spin allowed): the triplet oxygen atom O(^{3}P) and the triplet carbene molecule (Fig. 13(b)). The heterolytic cleavage needs much higher energy (270 kcal mol^{-1}, Fig. 13(c)). In contrast, the corresponding processes in the guanine anion are much easier. Thus, dissociation to the triplet oxygen atom O(^{3}P) and anion $C_5H_4N_5^-$ (135 amu) requires only 139 kcal mol^{-1} (Fig. 13(e)), which is 48 kcal mol^{-1} easier than for neutral molecules. This is in a qualitative agreement with observation of the anion of 134 amu mass.[36] The large values of dissociation energy do not correlate with the ion-yield cross-section peaks. Probably, the ions arise from formation of a dipole-bound anion in a vibrationally excited state, which couples to the $\sigma_{C=O}$* state. The dipole bound anion is arranged by the binding of the excess electron "sitting" on a diffuse orbital outside the molecular frame by the dipole moment of the polarized neutral molecule frame.[40] In such case the Feshbach resonance associated with dissociative vibration can be responsible for ion fragmentation and the bond rupture requires lower energy.

Since the NH_2 group and oxygen atom anions are indistinguishable by mass, the 16 amu peaks in the ion-yield spectra[36] can correspond to both species. Thus, the other opportunity can be connected with the NH_2 dissociation. Some low-energy features in the yield function[36] can be assigned to formation of the excited dipole-bound anions.[37] The dipole bound Feshbach resonance associated to the ν level of the N10–C2 stretching vibration coupled to the $\sigma_{N\text{-}H}$* state[40] can lead to the first peak in the guanine ion-yield spectrum.[33] The dipole bound nucleobase anions have been predicted[41,42] and observed in supersonic jet expansion experiments.[43] We calculated the dipole moment of guanine to be as much as

TABLE VII. Calculated energies of the starting reactants and products for the NH_2 elimination from guanine.

Fragment	Total energy, hartree
Guanine ^{1}G	– 542.3698309
Guanine anion ^{2}G$^-$	– 542.3161845
^{1}(G–NH_2)$^+$	– 486.0777217
^{2}(G–NH_2)	– 486.3344614
^{1}(G–NH_2)$^-$	– 486.3963136
^{2}(NH_2)	– 55.8529171
^{1}(NH_2)$^-$	– 55.8231872

7.2 D, while for adenine it is predicted to be equal to 2.48 D (in a good agreement with the data of Refs. 36 and 41). This is higher than the critical dipole moment of a molecule to form dipole-bound anion excited state.[36] But there are no obvious reasons to explain why dehydrogenation of adenine proceeds through creation of a dipole-bound state, and why this is not the case for guanine. Probably, dehydrogenation occurs via a simple core excited resonance.

From Table VII and the calculated reaction heat for the hemolytic (1), (2) and heterolytic NH_2 elimination (3), (4) from guanine molecule (1), (3) and from its anion (2), (4), one can see that production of the $(G–NH_2)^-$ mass (135 amu) is the most probable process. It is easier than the homolytic NH_2 elimination from the neutral guanine molecule by 72.5 kcal/mol. This is connected with a prolongation of the C2-N10 chemical bond by 0.059 Å upon electron attachment (the largest bond change upon anion generation). Homolysis of the guanine anion requires only 42 kcal mol^{-1} or 1.82 eV. This process can be efficient with simple core excitation and indicate quite strong scattering in our mass spectrum in Fig. 10. It corresponds to a very intense peak (135 amu mass) of the negative ion:[33]

Homolysis of neutral guanine

$$^1\mathrm{G} \rightarrow {}^2(\mathrm{G}-\mathrm{NH_2}) + {}^2(\mathrm{NH_2}) + 114.5\ \mathrm{kcal\ mol^{-1}}, \quad (2)$$

Homolysis of guanine anion

$$^2\mathrm{G}^- \rightarrow {}^1(\mathrm{G}-\mathrm{NH_2})^- + {}^2(\mathrm{NH_2}) + 42\ \mathrm{kcal\ mol^{-1}}, \quad (3)$$

Heterolysis of neutral guanine

$$^1\mathrm{G} \rightarrow {}^1(\mathrm{G}-\mathrm{NH_2})^+ + {}^1(\mathrm{NH_2})^- + 295\ \mathrm{kcal\ mol^{-1}}, \quad (4)$$

Heterolysis of guanine anion

$$^2\mathrm{G}^- \rightarrow {}^2(\mathrm{G}-\mathrm{NH_2}) + {}^1(\mathrm{NH_2})^- + 99\ \mathrm{kcal\ mol^{-1}}. \quad (5)$$

In fact, the electron affinity of the ^{2}(G–NH_2) radical ($\varepsilon^{\beta}_{LUMO}$ =3.56 eV) almost coincides with the value of the G-NH_2 dissociation energy (D = 3.9 eV[36]). Thus, this explains a strong drive of such a reaction which occurs almost at the appearance energy close to 0 eV.

The heterolytic cleavage with the $(NH_2)^-$ production (16 amu) is a much higher endothermic process (4). This is in agreement with a high-energy peak in the ion yield spectrum for such anion mass.[36] Comparison with the possible routs of oxygen elimination from the guanine anion (Fig. 13) clearly indicates that the mass (16 amu) can be assigned predominantly to amino anion.

The comparative study of low-energy electrons scattering data by adenine and guanine suggests that the latter is less sensitive to electron attacks. A detailed understanding of such low-energy electron collisions, their cross-sections and induced fragmentation features of the purines molecules (adenine and guanine) requires comparison of our measurements and theoretical data with results of previous investigations.[11,31–37] By comparison of Table VII and Fig. 13, one can conclude that the 135 amu negative fragment mass produced from guanine in the measurements of Ref. 36 can be attributed to reaction (2). In general either (G–O)– or (G–NH_2)– anions can be responsible for this mass. The formation of the former species would require much higher energy due to the double bond nature of the polarized C=O chemical feature. The DFT calculations (Table VII and Fig. 13) support the conclusion[36] that (G–NH_2)– is rather formed than (G–O)– in low-energy electron scattering by guanine molecule. Our cross-section (Fig. 10) can also be consistently interpreted on these backgrounds.

IV. CONCLUSIONS

Knowledge of the interaction between low-energy electrons and individual components of DNA can be useful for global analysis of the mechanisms of DNA radiation damage.[8] In this work, the crossed electron-molecular beams experiments have been presented and interpreted by the extensive DFT calculations in order to unravel the fragmentation mechanisms in the adenine and guanine cations and anions induced by electron impacts. Comparative ionization and fragmentation processes in these species are in general agreement with our DFT results.

The ionization cross-section by the 90 eV electron beam reaches about $(3.2 \pm 0.15) \times 10^{-15}$ cm^2 for guanine and is 10% higher than that for adenine. According to these cross-sections, the measured ionization threshold (8.3 eV) for the former molecule is lower by 0.5 eV in comparison with the adenine molecule. This difference between guanine and adenine ionization potentials (IP) can be well reproduced by all quantum chemical methods used in the present study (0.48 eV in DFT method). For all studied nucleobases,[6–10] we see a natural trend: the lower IP—the higher ionization cross-section maximum.

From comparison of the present results with previous measurements,[6–10,32–36] one can conclude that among all isolated nucleobases, uracile (U), thimine (T), adenine (A), guanine (G), and cytosine (C), the dissociative electron-attachment to guanine is the most specific one; it exhibits the wide shoulders on the negative ionization cross-section (Fig. 10) on the left and right sides from the main peak. Our DFT calculations and comparison with results of the anion yield mass spectra[32–36] provide some background for such

peculiarity of the G case. The other nucleobases (U, T, A, and C) also produce transient anions at low energy of bombarding electrons, while these anions eliminate mostly a neutral H atom (almost exclusively from the nitrogen positions[32–36] as it follows from our DFT calculation). For nucleobases coupled in the DNA network, this means that in the case of U, T, A, and C the base can act as an acceptor of low-energy electrons and this energy can be eventually transferred (via the N–H bond) to the DNA backbone inducing the strand breaks[44] (via hydrogen bonds cleavage). The variety of radicals produced at sub-excitation energy can induce complex chemistry also leading to strand breaks, initiating an avalanche effect. This can lead to genetic damages by intermediate radical attack on other sensitive DNA targets as phosphate residues, saccharides,[44] and peptide components in the biosynthesis processes.

ACKNOWLEDGMENTS

All computations were performed on resources provided by the Swedish National Infrastructure for Computing (SNIC) at the Parallel Computer Center (PDC) through the project "Multiphysics Modeling of Molecular Materials," SNIC 020/11-23. This research was also supported by the Ministry of Education and Science of Ukraine (Project No. 0113U001694).

[1] J. A. LaVerne and S. M. Pimblott, Radiat. Res. **141**, 208 (1995).
[2] V. Cobut, Y. Frongillo, J. P. Patau, T. Goulet, M. J. Fraser, and J. P. Jay-Gerin, Radiat. Phys. Chem. **51**, 229 (1998).
[3] L. Sanche and L. Parenteau, J. Chem. Phys. **93**, 7476 (1990).
[4] X. Pan, P. Cloutier, D. Hunting, and L. Sanche, Phys. Rev. Lett. **90**, 208102 (2003).
[5] S. Ptasinska and L. Sanche, J. Chem. Phys. **125**, 144713 (2006).
[6] I. I. Shafranyosh, M. I. Sukhoviya, and M. I. Shafranyosh, J. Phys. B. **39**, 4155 (2006).
[7] O. Boulanouar, M. Fromm, C. Mavon, P. Cloutier, and L. Sanche, J. Chem. Phys. **139**, 055101 (2013).
[8] I. I. Shafranyosh, V. V. Stetsovich, N. N. Chavarga, and M. I. Sukhoviya, Opt. Spectrosc. **112**, 155 (2012).
[9] I. I. Shafranyosh and M. I. Sukhoviya, J. Chem. Phys. **137**, 184303 (2012).
[10] I. I. Shafranyosh and M. I. Sukhoviya, Opt. Spectrosc. **102**, 500 (2007).
[11] D. Huber, M. Beikircher, S. Denifl, F. Zappa, S. Matejcik, A. Bacher, V. Grill, T. D. Mark, and P. Scheier, J. Chem. Phys. **125**, 084304 (2006).
[12] F. Trinter, M. S. Schöffler, H.-K. Kim, F. P. Sturm, K. Cole, N. Neumann, A. Vredenborg, J. Williams, I. Bocharova, R. Guillemin, M. Simon, A. Belkacem, A. L. Landers, Th. Weber, H. Schmidt-Böcking, R. Dörner, and T. Jahnke, Nature (London) **505**, 664 (2014).
[13] T. Jahnke, H. Sann, T. Havermeier, K. Kreidi, C. Stuck, M. Meckel, M. Schöffler, N. Neumann, R. Wallauer, S. Voss, A. Czasch, O. Jagutzki, A. Malakzadeh, F. Afaneh, Th. Weber, H. Schmidt-Böcking, and R. Dörner, Nat. Phys. **6**, 139 (2010).
[14] K. Gokhberg, P. Kolorenč, A. I. Kuleff, and L. S. Cederbaum, Nature (London) **505**, 661 (2014).
[15] A. D. Becke, J. Phys. Chem. **98**, 5648 (1993).
[16] M. J. Frisch, G. W. Trucks, H. B. Schlegel *et al.*, GAUSSIAN 09, Revision A.02, Gaussian, Inc., Wallingford, CT, 2009.
[17] M. J. S. Dewar, E. G. Zoebish, E. E. Headly and J. J. Stewart, J. Am. Chem. Soc. **107**, 3902 (1985).
[18] J. M. Rice and G. O. Dudek, J. Am. Chem. Soc. **89**, 2719 (1967).
[19] H. W. Jochims, M. Schwel, H. Baumgartel, and S. Leach, Chem. Phys. **314**, 263 (2005).
[20] A. N. Zavilopulo, O. P. Shpenik, and A. S. Agafonova, J. Phys. B. **42**, 025101 (2009).
[21] N. S. Hush and A. S. Cheung, Chem. Phys. Lett. **34**, 11 (1975).
[22] B. I. Verkin, L. F. Sukodub, and I. K. Yanson, Dokl. Akad. Nauk SSSR **228**, 1452 (1976).
[23] V. V. Afrosimov, A. A. Basalaev, Yu. G. Morozov, M. N. Panov, O. V. Smirnov, and E. A. Tropp, Tech. Phys. **57**, 594 (2012).
[24] J. Lin, C. Yu, S. Peng, I. Akiyama, K. Li, L. K. Lee and P. R. LeBreton, J. Am. Chem. Soc. **102**, 4627 (1980).
[25] S. K. Sethi, S. P. Gupta, E. E. Jenkins, C. W. Whitehead, L. B. Townsend, and J. A. McCloskey, J. Am. Chem. Soc. **104**, 3349 (1982).
[26] M. G. Barrio, D. I. C. Scopes, J. B. Holtwick, and N. J. Leonard, Proc. Natl. Acad. Sci. U.S.A. **78**, 3986 (1981).
[27] J. M. Rice, G. O. Dudek, and M. Barber, J. Am. Chem. Soc. **87**, 4569 (1965).
[28] C. Champion, J. Chem. Phys. **138**, 184306 (2013).
[29] J. L. McLain, C. D. Molek, D. Osborne, and N. C. Adams, Int. J. Mass Spectrom. **282**, 85 (2009).
[30] J. Semaniak, B. F. Minaev, A. V. Derkatch, F. Hellberg, A. Neau, R. Thomas, M. Larsson, H. Danared, A. Paal, and M. af Ugglas, Astrophys. J. Suppl. Ser. **135**, 275 (2001).
[31] P. Cheng, Y. Li, S. Li, M. Zhang, and Z. Zhou, Phys. Chem. Chem. Phys. **12**, 4667 (2010).
[32] E. C. M. Chen, J. R. Wiley, and E. S. Chen, Nucleosides, Nucleotides Nucleic Acids **27**, 506 (2008).
[33] K. Aflatooni, G. A. Gallup, and P. D. Burrows, J. Phys. Chem. **102**, 6205 (1998).
[34] K. Aflatooni, A. M. Csheer, and P. D. Burrows, J. Chem. Phys. **125**, 054301 (2006).
[35] H. Xie and Z. Cao, Int. J. Quantum Chem. **107**, 1261 (2007).
[36] H. Abdoul-Carime, J. Langer, M. A. Huels, and E. Illenberger, Eur. Phys. J. D **35**, 399 (2005).
[37] J. R. Wiley, J. M. Robinson, S. Ehdaie, E. C. M. Chen, E. S. D. Chen, and W. Wentworth, Biochem. Biophys. Res. Commun. **180**, 841.(1991).
[38] D. Volyniuk, V. Cherpak, P. Stakhira, B. F. Minaev, G. V. Baryshnikov, M. Chapran, A. Tomkeviciene, J. Keruckas, and J. V. Grazulevicius, J. Phys. Chem. C **117**, 22538 (2013).
[39] We consider that EA is positive if an electron attachment is the exothermic process. In terms of Koopmans theorem this means that the LUMO energy is negative.
[40] H. Abdoul-Carime, S. Gohlke, and E. Illenberger, J. Am. Chem. Soc. **126**, 12158 (2004).
[41] E. C. M. Chen and E. S. Chen, J. Phys. Chem. B **104**, 7835 (2000).
[42] R. L. Platzman, Radiat. Res. **17**, 419 (1962).
[43] C. Desfrançois, H. Abdoul-Carime and J.-P. Schermann, J. Chem. Phys. **104**, 7792 (1996).
[44] B. F. Minaev, Y. V. Yevtukhov, and V. A. Minaeva, Biopolym. Cell **21**, 351 (2005).
[45] See supplementary material at http://dx.doi.org/10.1063/1.4871881 for Figures S1–S5.